A RELATIVE COMPARISON OF NOISE PERFORMANCES BETWEEN DIFFERENT PMRI ALGORITHMS

Ifat Al Baqee

***Abstract*—**Parallel Magnetic Resonance imaging (pMRI) methods enable reduction of the acquisition rate via subsampled acquisitions of the k-space data. SENSE, GRAPPA, and iterative optimization-based methods are the most popular reconstruction approaches for modern MRI. The reconstruction processes can accumulate to a variance of noise value which is dependent on the position within the final image. Hence, estimating the noise accumulated during reconstruction is an integral part to judge a pMRI algorithm. In this paper, the noise performances of various popular pMRI algorithms have been estimated and compared. Geometry-factor or g-factor maps and standard deviations of the reconstructed final images by various state-of-the-art pMRI algorithms have been computed and compared which will provide an idea while nitpicking a particular method to optimize the noise performance for best-case scenario.

***Keywords*—**g-maps, standard deviations, GRAPPA, SENSE, SPIRiT, iterative optimization, convex optimization, sum-of-square, artifacts.

I. INTRODUCTION

THE augmentation of noise in parallel MRI (pMRI) reconstruction has always been an important issue in the parallel imaging community. Accelerated parallel MRI can be flogged by non-uniform noise during reconstruction. In this work, the efficiency of the several pMRI reconstruction algorithms is discussed based on their performances in case of noise enhancements. Additional noise is also going to add to the acquired dataset to observe and compare the quantitative performances of popular pMRI methods in noisy cases as well as the graphical comparison is going to be done with the help of geometry factor (g-factor) [1]-[2].

The reconstructed image by pMRI is complex and is proportional to the proton density of the object, the external magnetic field, and the radio frequency excitation pulses. The sensitivity functions of the scanner coils are also complex-valued [3]. The pMRI reconstruction is based on the under-sampled k-space (Fourier) data and requires knowledge of the coil sensitivity functions. There have been several pMRI methods established in past years for final image acquisition. Depending on how the information of sensitivity functions is processed and incorporated into the image reconstruction, the existing reconstruction algorithms may be classified into three groups.

The first group of algorithms pre-estimates the coil sensitivity functions using a pre-scan [4]. Typical algorithms of this cluster are SMASH [5], SENSE [4], and their extensions such as [6]-[8]. Accuracy of pre-estimated sensitivity functions is essential, which is difficult to achieve in practical measurements. The second group of pMRI reconstruction algorithms is based coil-by-coil reconstruction method and the sum-of-squares (SOS) operation [3]. Explicit values of the sensitivity functions are not required in the auto-calibration based algorithms. Typical methods of this group are GRAPPA [9], IIR GRAPPA [10], and their extensions, which carry out interpolation to recover the missing samples. The third genre of algorithms formulates the pMRI reconstruction into an iterative regularized optimization problem. These algorithms jointly determine the image and coil sensitivity functions by minimizing a performance index function that incorporates the reconstruction error and regularization terms [11]-[15], [16], [17]. Among these three classes of algorithms, JSENSE from the first group; GRAPPA [9], SPIRiT [18] and ESPIRiT [19] from the second group; IRGN-TGV [15], Dual-step convex optimization [16] and single-step convex optimization [17] from the third group has been chosen to estimate their g-factor maps and standard deviation to compare noise performances. Hopefully, the comparison results will provide a comprehensive idea to readers about the noise efficiency of different algorithms.

II. THEORY AND METHODOLOGY

The signal-to-noise ratio (SNR) in MRI is an important aspect of performance measurement. After the arrival of multiple coil arrays, significant improvement in fundamental SNR performance had been observed in parallel MRI (pMRI) reconstruction. However, pMRI has also come with a drawback of introducing non-uniform SNR in the final reconstructed image [1], [20]. Also, SNR is inversely proportional to

I. A. Baqee is with the Department of Electrical and Electronic Engineering, Southeast University, Tejgaon, Dhaka 1208, Bangladesh (e-mail: *ifat.albaqee@seu.edu.bd*).

the square root of the reduction factor [1].

Another element that affects the SNR performance in parallel imaging is the coil geometry which is also known as the g-factor. The geometry factor or g-factor depicts the noise enhancement in pMRI reconstruction which is spatially dependent and proportionally incremental to the square root of reduction factor as well as strongly connected to the encoding efficiency of receiver coils.

Over the past few years, many algorithm-depended analytical procedures have been proposed to estimate the g-factor for pMRI reconstructions. Sensitivity based methods like SENSE and SMASH applied Kellman and McVeigh's [21] method to determine SNR and hence g-factor. Yeh in [22] also provided a general outline to estimate g-factor for PARS (Parallel magnetic resonance imaging with adaptive radius in k-space) based reconstructions. Several techniques have also been proposed to calculate g-factor for auto-calibration based methods such as GRAPPA, in [1], [23], [24]. Although, the typical standard way to derive g-factor is from a set of fully acquired series of datasets with identical scanning parameters and conditions. From these series of datasets, SNR maps are derived which is the ratio of mean and standard deviation measurements on a pixel-by-pixel basis of the reconstructed images from the fully sampled datasets. Then the datasets are under-sampled by manually removing some of the phase encoding k-space lines and reconstructed followed by the estimation of accelerated SNR from the mean and standard deviation of the reconstructed images on a pixel-by-pixel basis. The non-uniform noise enhancement factor or simply the g-factor is derived from the ratio of SNR of from fully sampled datasets and accelerated SNR multiplied by the square root of the reduction factor [1].

$$\varsigma = \frac{SNR^{full}}{SNR^{acc}\sqrt{f_{net}}} \tag{1}$$

where ς denotes the g-factor, SNR^{full} is the signal-to-noise ratio derived from the fully sampled set of datasets, SNR^{acc} is derived from accelerated under-sampled datasets and f_{net} is the net acceleration or reduction factor. Let h_m is the reconstructed image from an under-sampled dataset and h_{SOS} is the reconstructed reference image from the fully acquired dataset. The SNR for the reconstructed images from fully acquired datasets and under-sampled datasets by

$$SNR_p^{full} = \frac{\hat{h}_{SOS_p}}{\bar{h}_{SOS_p}} \tag{2}$$

where p denotes the pixel index. $\hat{h}_{SOS_p}$ is the mean value for the reconstructed images from fully sampled J sets of datasets.

$$\hat{h}_{SOS_p} = \frac{1}{J}\sum_{j=1}^{J} h_{SOS_p}(j) \tag{3}$$

$\bar{h}_{SOS_p}$ is the standard deviation for the images from fully acquired datasets.

$$\bar{h}_{SOS_p} = \sqrt{\frac{1}{J}\sum_{j=1}^{J}\{h_{SOS_p}(j) - \hat{h}_{SOS_p}\}^2} \tag{4}$$

Same equations have been used to derive mean and standard deviations for manually under-sampled reconstructed images to estimate SNR_p^{acc}.

However, to provide a more precise estimation of the g-factor maps, at least 100 scanned datasets are recommended [1] to perform pMRI reconstruction to get images from both fully sampled datasets and under-sampled datasets which are used to calculate SNR_p^{full} and SNR_p^{acc}. Some recent methods like [24] and [25] can estimate SNR maps from one fully sampled dataset and one additional noise only dataset, but their applicability is limited to objects in motion. Obtaining such large sets of data through scanning is time-consuming as well as performing isolated pMRI reconstruction for each set of data. This time limitation makes the experimental procedures be applied to limited types of datasets.

III. Experimental Set-up and Results

Two sets of datasets have been acquired to generate g-factor maps for the proposed optimization methods in this work. First, is an in-vivo brain dataset already been used to test the efficiency of the proposed methods in this work, additive Gaussian noises with different variances have been mixed with the dataset to produce several sets of contaminated datasets with varying noises. These datasets are applied to generate simulated g maps (as these are not obtained 100 times through separate scanning using similar parameters) for the proposed methods as well as some popular state-of-art methods. Normalized mean square errors (NMSE) have been also calculated for each set and averaged to make comparisons between the proposed optimization algorithms and some nominated state-of-art algorithms. As mentioned earlier, seven state-of-the-art methods have been nominated to compare the noise performances; GRAPPA, SPIRiT, ESPIRiT, IRGN-TGV, JSENSE, Two-step convex optimization method, and direct convex optimization method. It is also worth mentioning to the readers that the last two pMRI reconstruction algorithms are from the author's previous research work.

A. Data Acquisition

The first dataset is a single slice brain data set of a

healthy human volunteer available in [26], which was acquired by a 3 Tesla SIEMENS Trio scanner with an eight-channel head array and an MPRAGE (3D Flash with IR prep.) sequence. The parameters of the scan were TR/TE = 2530/3.45 ms, TI = 1100 ms, flip angle = 7^0, image size is 256 by 256, slice thickness = 1.33 mm and FOV = 256 by 256 mm^2. The fully acquired k-space data are manually and uniformly under-sampled at the nominal acceleration rate, denoted by f_{nom}, together with an additional 36 extra auto-calibration signal (ACS) lines in the central k-space region along the phase encoding direction to form the under-sampled k-space data pattern. Four sets of under-sampled data at f_{nom} = 4, 8, 12, and 16 have been obtained. Taking into account the additional 36 ACS lines, the corresponding net under sampling rates, denoted by f_{net}, of the datasets are f_{net} = 2.56, 3.76, 4.49 and 4.92, respectively. To evaluate the reconstruction performance subject to measurement noise and varying noisy conditions, 50 random noise vectors were generated with a uniform magnitude increment of 20%. The noise vector is Gaussian noise in nature with zero mean and variance of 1.53%. In the performance evaluation subject to noise, each of the 50 noise vectors was Fourier transformed to k-space data and manually added to the fully sampled k-space data followed by the under-sampling and reconstruction processes.

The second one is a phantom which was scanned for 100 times and was acquired on a 3 Tesla SIEMENS scanner with a 32-channel head with true fast imaging with steady-state precession sequence (TrueFISP). The parameters of the scan were TR/T E = 11/6.5 ms, N×N = 256 × 256, flip angle = 60^0 and FOV = 162 × 162 mm^2. The acquired k-space data is in the Cartesian coordinate system and uniformly under-sampled at the nominal rate of f_{nom} = 4 and 8. The undersampled data together with the 32 extra ACS lines in the central k-space region along the phase encoding direction generating an under-sampled k-space dataset with a net under sampling rate f_{net}= 2.67 and 4.

B. Computational Setups

All the computational algorithms for pMRI reconstructions have been programmed by MATLAB (Math-Works, Natick, MA, USA). the normalized mean square error of the reconstructed image h_m is defined as

$$e_{NMSE} = \frac{\|h_m - h_{SOS}\|^2}{\|h_{SOS}\|^2} \quad (5)$$

The reconstructed g-factor maps by the proposed algorithms have been computed and compared with some selected state-of-art reconstruction algorithms under the same data acceleration factors. Specifically, the simulated g-maps from 50 sets of brain images reconstructed for different additive noises at aforementioned under sampling rates are compared with that reconstructed by the conjugate gradient SPIRiT (CG SPIRiT) with L1 penalty, GRAPPA, L1 ESPIRiT, IRGN-TGV, JSENSE, Two-step convex optimization, and direct convex optimization algorithms. The g-factor maps resulted from the phantom, which was scanned 100 times to provide a more accurate result, are compared with GRAPPA and L1 ESPIRiT. Due to the time-consuming factor associated with the reconstruction of a such number of images, some of the time-consuming methods used for comparison earlier are escaped in this g-map analysis between different algorithms. The MATLAB codes as well as the regularization parameters and initial conditions for computations of these algorithms are set by the theory and methods narrated by the respective authors.

C. Results and Analysis

The g-factor maps estimated for an acceleration factor of f_{nom} = 8 for different algorithms are displayed in Fig. 1.

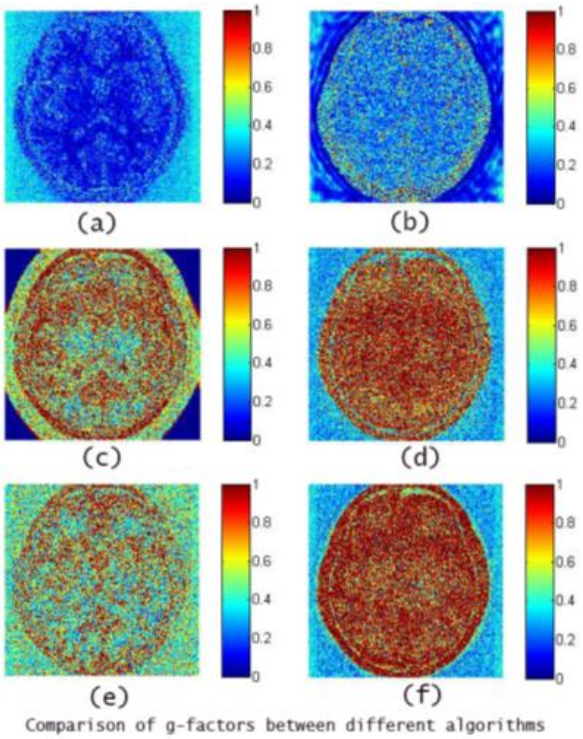

Fig. 1. g-factor maps reconstructed for the 8-channel brain data set at by the two-step optimization algorithm in (a), IRGN-TGV in (b), l1 ESPIRiT in (c), CG-SPIRiT in (d), JSENSE in (e) and GRAPPA in (f) respectively

As g-maps depict the noise enhancement factor for each reconstruction algorithm, it is clear from the figure that the proposed two-step convex optimizations algorithm in Fig. 1 (a) demonstrates the best outcome among the selected algorithms in case of reconstruction

noise suppressing capability, followed by IRGN-TGV in Fig. 1 (b). Coil-by-coil reconstruction methods like ESPIRiT, SPIRiT, and GRAPPA which employ SOS for final image reconstruction, exhibit more noise amplifications. ESPIRiT in Fig. 1 (c), also tends to be more insusceptible to noise enhancement among other similar algorithms but still falling behind the first and third category of algorithms.

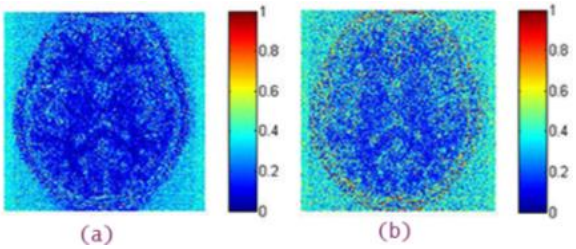

Fig. 2. g-factor maps reconstructed for the 8-channel brain data set at by the two-step optimization algorithm in (a), Direct optimization method in (b) respectively

Fig. 2 represents a comparison of g-maps between the two-step and direct algorithms. This figure illustrates that the direct optimization method exhibits more reconstruction noise enhancement. Also, when compared to the g-map by IRGN-TGV at Fig. 1 (b), it displays a higher magnitude of noise outside of the actual image of the slice but a lower noise enhancement inside the actual image area. Although, it should be noted that the noise enhancement factor cannot define the quality of reconstruction alone but sometimes more noise reduction can lead to loss of details in the actual reconstructed image.

TABLE I
AVERAGED NMSE VALUES OF 50 BRAIN IMAGES RECONSTRUCTED BY DIFFERENT ALGORITHMS SUBJECT TO NOISE

f_{nom}	4	8	12	16
GRAPPA	0.0082	0.0133	0.0215	0.0341
SPIRIT	0.0078	0.0125	0.0196	0.0287
ESPIRIT	0.0068	0.0104	0.0156	0.0225
IRGN-TGV	0.0045	0.0069	0.0086	0.0112
JSENSE	0.0085	0.0102	0.0169	0.0208
TWO-STEP METHOD	0.0038	0.0053	0.0071	0.0098
DIRECT METHOD	0.0036	0.0055	0.0076	0.0105

TABLE II
STANDARD DEVIATIONS (%) OF RECONSTRUCTED IMAGES FROM 50 BRAIN IMAGES BY DIFFERENT ALGORITHMS SUBJECT TO NOISE

f_{nom}	4	8	12	16
GRAPPA	0.91	1.09	1.69	2.27
SPIRIT	0.88	1.05	1.60	2.07
ESPIRIT	0.44	0.72	1.01	1.46
IRGN-TGV	0.11	0.18	0.36	0.58
JSENSE	0.21	0.34	0.49	0.65
TWO-STEP METHOD	0.11	0.16	0.33	0.53
DIRECT METHOD	0.10	0.17	0.32	0.59

*Lower is Better

Finally, the average of the NMSE values of the 50 images reconstructed by each different algorithm and the standard deviations of the NMSE values of the 50 reconstructed images by each algorithm is summarized in Table I and Table II, respectively.

From the results of in vivo brain data, it is observed that the second category of algorithms, which employs SOS after coil-by-coil reconstructions, tend to exhibit more noise than others. This is due to the fact that these methods assume that coil sensitivities are uniform and hence depend less on it. Practically, coil data may be plagued by inhomogeneities of MR machines and often yields non-uniform sensitivity functions. Meanwhile, SENSE-based methods like JSENSE compute the coil functions explicitly which may result in less noise accumulate. Iterative methods like IRGN, Two-step convex optimization, and Direct optimization use noise minimizing TV penalties, which gives that great advantage in case of noise performance.

g-factor maps have been also estimated for the acquired 100 sets of phantom data which can give a more accurate idea about the noise enhancement factor of the proposed convex optimization-based algorithms. ESPIRiT and GRAPPA have been chosen to compare the noise amplification performance with the proposed algorithms in this research. Methods like JSENSE, IRGNTGV, Sparse-BLIP, and CS-SENSE have been escaped for comparison due to their long time consumption to perform the pMRI reconstruction, which makes the g-maps construction from the 100 sets of scanned data devouring extensive time and those methods to be out of consideration.

The g-maps resulted from the 100 scanned phantom datasets for the selected algorithms are shown in Fig. 3 for a nominal acceleration rate of f_{nom} = 4 (f_{net} = 2.67). In the figure, a brighter image corresponds to more noise enhancement. From the figure, it is cleared that except GRAPPA, all other methods perform quite well. The two-step method by convex optimizations in Fig. 3(a) (a) accomplishes the best result. Although noise enhancement by direct optimization method, shown in Fig. 3(b), is also on the lower side but few pixels consisting of higher noise data can be observed. g -map resulted by SPIRiT in Fig. 3(c), is also very smooth but brighter image than Fig. 3(a) and 3(b) means overall noise amplification is a little bit higher.

The g-factor maps stemmed from a nominal acceleration rate of f_{nom} = 8 (f_{net} = 4), by various methods have been displayed in Fig. 7.4. As expected, the noise amplification has been increased for each of the selected algorithms as the reduction factor has also been increased. Again, except GRAPPA, all other algorithms have handled reconstruction noise well and the differences between these are subtle. But upon closer inspection it can be seen that the g-map from the

two-step method in Fig. 4(a) offers less noise, closely followed by the result of the direct optimization method in Fig. 4(b) and ESPIRiT in Fig. 4(c). The comparisons using the phantom data has also established the facts that have been discussed earlier. These simulation results from phantom data have been consisted of in vivo brain data. pMRI algorithms that depend implicitly on coil functions often exhibit a higher amount of reconstruction noises as these are based on the fact that coil functions are always uniform. Also, it is noted that newer methods in this group as ESPIRiT performs better than older algorithms. Iterative methods have the upper hand on noise performance because noise minimizing penalties like TV norm can be applied [15].

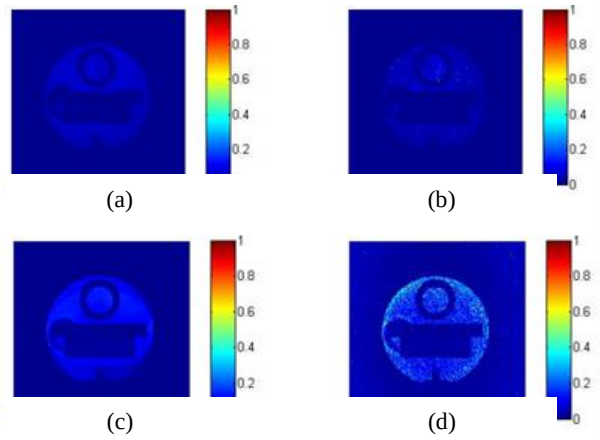

Fig. 3. Reconstructed g-factor maps from the 100 phantom datasets at $f_{nom} = 4$ by the two-step optimization algorithm in (a), direct optimization method in (b), l1 ESPIRiT in (c), GRAPPA in (d) respectively

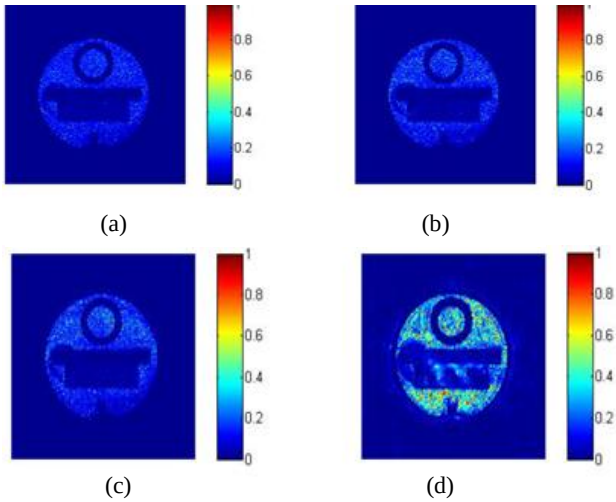

Fig. 4. Reconstructed g-factor maps from the 100 phantom datasets at $f_{nom} = 8$, by the two-step optimization algorithm in (a), direct optimization method in (b), l1 ESPIRiT in (c), GRAPPA in (d) respectively

IV. Conclusion

Parallel MRI methods have been known to introduce non-uniform noise in the reconstruction of MR image and to study noise amplification in pMRI reconstruction has been an interesting topic which can provide some knowledge on how well an algorithm can treat noise enhancement during reconstruction. For that, g-factor has been standardized as the primary parameter to measure noise enhancements for pMRI methods. The purpose of this work has been to analyze the noise enhancement factor resulted from popular pMRI algorithms and to compare them thoroughly with some standard parameters like g-factor maps. The efficiency and accuracy of the algorithms in case of added noise to the acquired k-space data have also been evaluated and shown in this paper. Graphical, as well as numerical comparisons have been done in detail to represent the effectiveness of the various algorithms in case of handling and acquainting noise during reconstructions compared to other methods. From the experimental figures and numerical scrutiny, it is obvious that the two-step method by convex optimizations and direct convex optimization method is very efficient in noise enhancement management. Also, these comparisons give researchers a clue about the prospect of iterative optimization algorithms for pMRI reconstruction.

References

[1] F. A. Breuer, S. A. Kannengiesser, M. Blaimer, N. Seiberlich, P. M. Jakob, and M. A. Griswold, "General Formulation for Quantitative Gfactor Calculation in GRAPPA Reconstructions," Magnetic Resonance in Medicine, vol. 62, pp. 739–746, 2009.

[2] S. Aja-Fernández, G. Vegas-Sánchez-Ferrero, and A. Tristán-Vega, "Noise estimation in parallel MRI: GRAPPA and SENSE," Magnetic Resonance Imaging, vol. 32, pp. 281–290, 2014.

[3] P. B. Roemer, W. A. Edelstein, C. E. Hayes, S. P. Souza, and O. M. Mueller, "The NMR Phased Array," Magnetic Resonance in Medicine, vol. 16, pp. 192–225, 1990.

[4] K. P. Pruessmann, M. Weiger, M. B. Scheidegger, and P. Boesiger, "SENSE: Sensitivity encoding for fast MRI," Magnetic Resonance in Medicine, vol. 42, pp. 952–962, 1999.

[5] D. K. Sodickson and W. J. Manning, "Simultaneous acquisition of spatial harmonics (SMASH): Fast imaging with radiofrequency coil arrays," Magnetic Resonance in Medicine, vol. 38, pp. 591–603, 1997.

[6] W. Kyriakos, L. Panych, D. Kacher, C. Westin, S. Bao, R. Mulkern, and F. Jolesz, "Sensitivity profiles from an array of coils for encoding and reconstruction in parallel (SPACE RIP)," Magnetic Resonance in Medicine, vol. 44(2), pp. 301–308, 2000.

[7] C. Liu, R. Bammer, and M. Moseley, "Parallel imaging reconstruction for arbitrary trajectories using k-space sparse matrices (kSPA)," Magnetic Resonance in Medicine, vol. 58, pp. 1171–1181, 2007.

[8] B. Madore, "UNFOLD-SENSE: a parallel MRI method with self-calibration and artifact suppression," Magnetic Resonance in Medicine, vol. 52, pp. 310–320, 2004.

[9] M. Griswold, P. Jakob, R. Heidemann, M. Nittka, V. Jellus, J. Wang, B. Kiefer, and A. Haase, "Generalized Autocalibrating Partially Parallel Acquisitions (GRAPPA)," Magnetic Resonance in Medicine, vol. 47, pp. 1202–1210, 2002.

[10] Z. Chen, J. Zhang, R. Yang, P. Kellman, L. A. Johnston, and G. F. Egan, "IIR GRAPPA for Parallel MR Image Reconstruction," Magnetic Resonance in Medicine, vol. 63, pp. 502–509, 2010.
[11] L. Ying and J. Sheng, "Joint image reconstruction and sensitivity estimation in SENSE (JSENSE)," Magnetic Resonance in Medicine, vol. 57, pp. 1196–1202, 2007.
[12] M. Uecker, T. Hohage, K. T. Block, and J. Frahm, "Image reconstruction by regularized nonlinear inversion – Joint estimation of coil sensitivities and image content," Magnetic Resonance in Medicine, vol. 60, pp. 674–682, 2008.
[13] H. She, R. Chen, D. Liang, Y. Chang, and L. Ying, "Image Reconstruction From Phased-Array MRI Data Based on Multichannel Blind Deconvolution," in Proc. 7th IEEE International Symposium on Biomedical Imaging: From Nano to Macro, 2010, pp. 760–763.
[14] D. Gol and L. C. Potter, "Ambiguity and Regularization in Parallel MRI," in 33rd Annual International Conference of the IEEE Engineering-in-Medicine-and-Biology-Society (EMBS), 2011, pp. 2829–2832.
[15] F. Knoll, C. Clason, K. Bredies, M. Uecker, and R. Stollberger, "Parallel imaging with nonlinear reconstruction using variational penalties," Magnetic Resonance in Medicine, vol. 67, pp. 34–41, 2012.
[16] Cishen Zhang and Ifat-Al-Baqee, "Parallel magnetic resonance imaging reconstruction by convex optimization", 2013 Third International Conference on Innovative Computing Technology (INTECH)in LONDON (IEEE Xplore), pp. 473-478, 2013.
[17] Ifat-Al-Baqee, Cishen Zhang and Xin GAO, "Optimal parallel MRI reconstruction over a convex solution space", 2015 IEEE International Conference on Signal Processing, Communications and Computing (ICSPCC), pp. 736-739, 2015.
[18] M. Lustig and J. M. Pauly, "SPIRiT: Iterative Self-consistent Parallel Imaging Reconstruction From Arbitrary k-Space," Magnetic Resonance in Medicine, vol. 64, pp. 457–471, 2010.
[19] M. Uecker, P. Lai, M. J. Murphy, P. Virtue, M. Elad, J. M. Pauly, S. S. Vasanawala, and M. Lustig, "ESPIRiT-An Eigenvalue Approach to Autocalibrating Parallel MRI: Where SENSE Meets GRAPPA," Magnetic Resonance in Medicine, vol. 71, pp. 990–1001, 2014.
[20] K. Zhu, "General Formulation for Quantitative G-factor Calculation in GRAPPA Reconstructions," *http://mrsrl.stanford.edu/www/studygroup/presentations/GRAPPA_G-factor_studyGroup_KangrongZhu_20110819.pdf*.
[21] P. Kellman and E. R. McVeigh, "Image reconstruction in SNR units: a general method for SNR measurement," Magnetic Resonance in Medicine, vol. 58, pp. 211–212, 2005.
[22] E. N. Yeh, C. A. McKenzie, M. A. Ohliger, and D. K. Sodickson, " Parallel magnetic resonance imaging with adaptive radius in k-space (PARS):constrained image reconstruction using k-space locality in radio frequency coil encoded data," Magnetic Resonance in Medicine, vol. 53, pp. 1383–1392, 2005.
[23] J. Wang, B. Zhang, K. Zhong, and Y. Zhuo, "Image Domain Based Fast GRAPPA Reconstruction and relative SNR degradation Factor," 2005, p. 2428, Magnetic Resonance in Medicine.
[24] P. M. Robson, A. K. Grant, A. J. Madhuranthakam, R. Lattanzi, D. K. Sodickson, and C. A. McKenzie, "Universal approach to quantification of SNR and g-factor for parallel MRI," 2007, p. 1747, In: Proc 15th Annual Meeting ISMRM, Berlin.
[25] M. J. Riffe, M. Blaimer, K. J. Barkauskas, J. L. Duerk, and M. A. Griswold, "SNR estimation in fast dynamic imaging using bootstrapped statistics," 2007, p. 1879, In: Proc 15th Annual Meeting ISMRM, Berlin.
[26] "Cartesian Dataset of Human Brain," *http://maki.bme.ntu.edu.tw*, 2005 (accessed in September 2019).

Ifat A. Baqee was born in Dhaka, Bangladesh. Dr. Baqee completed his Bachelor of Science (B.Sc.) in Electrical, Electronic and Communication Engineering from Military Institute of Science and Technology (MIST), Mirpur, Dhaka under Bangladesh University of Professionals (BUP) in February 2009. After that Dr. Baqee completed his Doctor of Philosophy (PhD) from the Swinburne University of Technology, Australia in 2016. The author's major field of study during the PhD tenure was computational image processing in the medical domain.

After graduation, he first joined as a Lecturer at Stamford University Bangladesh in 2009. He served there up to 2012. After that, he moved to Australia to pursue his PhD degree. After completion of PhD, he came back to Bangladesh and joined as an Assistant Professor at the American International University Bangladesh (AIUB), Dhaka. He served up to 2019 in AIUB and then joined Southeast University, Tejgaon, Dhaka, Bangladesh. He is currently serving there as an Assistant Professor in the EEE Department. His previous and current research interests include but are not limited to computational image processing, neural processing, medical instrumentation, power system automation, control system, etc. He has a good number of international journal and conference paper publications under his name.

Dr. Baqee is currently a member of the International Association of Computer Science and Information Technology (IACSIT). Dr. Baqee is also an active editorial member of the Australian Journal of Engineering and Innovative Technology (AJEIT).